Performance and dynamics of a novel bistable vibration energy harvester with appended nonlinear elastic boundary

Xuefeng Li[1], Daniil Yurchenko[2], Renfu Li[1*], Xingxing Feng [3], Bo Yan[4], Kai Yang[1*]

1. School of Aerospace Engineering, Huazhong University of Science and Technology, Wuhan 430074, China

2. Institute of Sound and Vibration Research, University of Southampton, Southampton, SO17 1BJ, UK

3. The 8th Research Laboratory, Wuhan 2nd Ship Design and Research Institute, Wuhan 430064, China

4. School of Mechanical Engineering and Automation, Zhejiang Sci-Tech University, Hangzhou, 310018, China

*Corresponding author: Renfu Li email: renfu.li@hust.edu.cn

*Corresponding author: Kai Yang email: kaiyang@hust.edu.cn

Abstract.

This paper proposes a novel bistable energy harvester coupled with a nonlinear elastic boundary (BEH-NB) to enhance energy harvesting performance. The analytical model of BEH-NB is derived and verified experimentally. Then the performance of the bistable energy harvester with different boundary conditions is investigated, including the bistable energy harvester with linear elastic boundary (BEH-LB), the bistable energy harvester without elastic boundary (BEH), and a linear energy harvester (LEH). The compared results show that the performance of BEH-NB is better than that of its counterparts. Results of the studied case show that the average power of BEH-NB can be improved by 42.05%, and the operational bandwidth is significantly widened by 93.18%, which is highly beneficial for energy harvesting. To identify the optimal parameters set for energy harvesting from ambient excitation, bifurcation analyses are performed. It is found that small changes in parameters can profoundly alter the system's steady-state response. The initial conditions also have a significant effect on the type of the system's response. Therefore, the basin of attraction of BEH-NB is calculated to reveal the influence of the initial conditions and to quantify the occurrence probability

of the different types of motion. The results of this paper provide a novel perspective in the structural design of the system and offer a practical application design guidelines to improve the system's performance.

Key Words: Energy harvesting; Nonlinear elastic boundary; Bistable nonlinearity; Bifurcation analyses; Basin of attraction

1. Introduction

Harvesting ambient vibration energy has attracted great attention in recent decades due to its environmentally friendly nature and sustainability. It can convert the ambient vibration energy into electrical energy for electronic devices [1-4]. There are several transduction mechanisms, such as electromagnetic [5-7], piezoelectric [8-10], and electrostatic [11]. Many technologies and concepts related to vibration energy harvesters (VEH) have been proposed due to their great potential and a wide range of applications [12,13]. A primitive energy harvester is based on a linear structure for absorbing energy of ambient vibration. It is effective only within a narrow bandwidth close to the resonant frequency, whereas the ambient vibration frequency range is often rather wide. Thus, a number of practical application scenarios for linear energy harvesters is very limited. Therefore, energy harvesters with wider resonance bandwidths are in great demand.

To broaden the effective bandwidth, nonlinearity has been introduced into the design of energy harvesters, including inter alia bistable nonlinearity [14-21], tristable nonlinearity [22-26], and quad-stable nonlinearity [27,28], etc., which have also been widely used in vibration isolation [29-34]. Zhou et al. [16] proposed a bistable nonlinear energy harvester, and experimental results demonstrate that the bistable nonlinearity can significantly improve the energy harvesting performance. Hou et al. [17] designed a bistable energy harvester that uses the change of a spring torque direction. They experimentally demonstrated that the bistable structure exhibited an increase in operational bandwidth and an improvement in output power. Li et al. [18] conducted a comprehensive study of the dynamic responses of the bistable energy harvester under filtered band-limited stochastic excitation. Results indicate that the bistable energy harvester can notably enhance energy harvesting performance. Lan and Qin [19] proposed a novel bistable energy harvester by adding a small magnet in the middle of the two

fixed magnets. It is proved that the performance of the bistable energy harvester is improved by adding an additional magnet to reduce potential barriers. Apart from the study of bistable energy harvesters, the tristable and quad-stable energy harvesters have also been studied recently. Sun et al. [23] proposed a novel tristable energy harvester and obtain the corresponding bistable state and monostable state by varying the magnet distance. The results showed that the output performance under the bistable state is better than that under the tristable state when the excitation is small, while the output performance under the tristable state is better than that under the bistable state when the excitation is large enough. The latest developments in multistable energy harvesting systems can be consulted in [35-37]. It is seen that achieving multiple stable equilibrium points for energy harvesters, such as tristable, quad-stable equilibrium points, requires high complexity of the structural design. On the other hand, the current design is hard to arbitrarily specify the coordinates of multiple equilibrium points, which is not conducive to optimizing the performance of the energy harvester. Therefore, the bistable energy harvester is the most representative one.

To improve the performance of bistable energy harvester, combing the multi-degree-of-freedom (multi-DOF) is a promising way to achieve higher energy harvesting performance. Recent studies have shown that multi-DOF may introduce new dynamic behaviors and thus improve the performance of energy harvester [18,38-44]. Harne et al. [38] comprehensively investigated the dynamics of the bistable energy harvester appended a degree of freedom. They found experimentally that the additional DOF can motivate a beneficial snap-through motion. This demonstrated that combining multi-DOF is a practicable way to enhance energy harvesting performance. Fan et al. [39] presented a 2DOF wideband energy harvester with magnetic coupling effect, which can reduce the potential barrier and effectively broaden the operational bandwidth. Nguyen et al. [40] indicated that the operational bandwidth of the 2DOF energy harvester can be doubled compare to a single-DOF energy harvester under reasonably strong intensity excitation. Due to the frequency distribution of ambient vibration being relatively wide, a larger operational bandwidth implicates better energy harvesting performance. This illustrates that the multi-DOF energy harvester has strong flexibility and environmental adaptability and can be applied to diverse scenarios.

Furthermore, some researchers have attempted to improve performance of energy harvesters by changing the boundary conditions through bio-inspiration [45-49]. Harne and Wang [46] designed a similar bistable structure with elastic boundary inspired by the skeleton of dipteran wings to implement a flapping wing mechanism. The research results show that the bistable oscillator with elastic boundary can achieve larger vibration amplitude under certain harmonic excitation, which also implies better energy harvesting performance. Zhang et al. [47] proposed an electromagnetic bistable energy harvester with linear elastic boundary (BEH-LB). The bistable energy harvester without elastic boundary (BEH) as a counterpart. It is found that the vertically attached linear elastic boundary helps to reduce the potential barrier and enhance the inter-well response.

The previous literature on bistable energy harvesters with linear elastic boundary corroborated the superiority of coupled dynamics due to bistable nonlinearity and linear elastic boundary [47]. It is noteworthy that the linear elastic boundary is a functional structure to enhance the snap-through oscillation of the bistable oscillator. But there is some defect that the the stiffness of the linear elastic boundary diminishes the bistability of the bistable oscillator. This limits the performance of the oscillator to exhibit large snap-through oscillations. However, the energy harvester with a nonlinear elastic boundary may be a viable technical path. This will potentially improve the energy harvesting performance by combining two nonlinear dynamic properties. Therefore, due to the wide application potential in low frequency energy harvesting, this paper proposes a novel bistable energy harvester with a nonlinear elastic boundary (BEH-NB), which is proposed and unexplored. To shed light on the beneficial effects of the nonlinear elastic boundary on targeted energy conversion from the excited nonlinear oscillator. This paper will compare the performance of the energy harvesters with different boundary conditions. Then, in order to deeply understand the nonlinear features of the BEH-NB, this paper will comprehensively investigate the dynamics of BEH-NB, which also provides a guide for the application of the BEH-NB.

The rest of this paper is organized as follows. In section 2, the analytical model of the BEH-NB is formulated. In section 3, experiments are carried out to validate the analytical model. In section 4, the performance of BEH-NB and its counterparts are contrasted. Section 5 performs bifurcation analyses to reveal the nonlinear behaviors of the BEH-NB. Section 6 sheds

light on the influence of the initial conditions on the responses of the BEH-NB, where the probability of occurrence of different steady-state response is also shown. Finally, Section 7 presents the main conclusions of this paper.

2. Analytical modeling of the BEH-NB

A structural model of a bistable electromagnetic energy harvester with a nonlinear elastic boundary (BEH-NB) is proposed as shown in Fig. 1, which consists of a stator, a horizontal oscillator, an inclined spring, and an adjustable nonlinear elastic boundary. The stator is a frame including a linear sliding chute with coils, which are connected to the resistor R. The horizontal oscillator m_1 is an embedded permanent magnet and a hinge fixed to it. The m_1 slides on the linear sliding chute with the linear damping constant c_1. The m_1 will convert the vibration energy into electric energy through an electromagnetic mechanism, which will be consumed by the resistor R. The inclined spring is a linear spring with stiffness k_1 having undeformed length l_1. The adjustable nonlinear elastic boundary consists of a vertical oscillator m_2, a vertical linear spring with stiffness k_2 having undeformed length l_2 and two horizontal linear springs with same stiffness k_3 having undeformed length l_3. The vertical oscillator m_2 slides on the vertical sliding chute with the linear damping coefficient c_2. One end of the inclined spring suspends m_1, while the opposing end connects to m_2. The vertical distance from m_2 to m_1 is h, where $h < l_1$. As a result, the inclined spring is compressed at the centerline position, thus forcing the oscillator to move away from the centerline and stop at two stable equilibrium positions symmetrical about the centerline, i.e., the bistable nonlinearity. The BEH-NB is excited through base excitation $\ddot{z}$, x is the relative displacement of m_1 to the centerline and positive to the right, y is the relative displacement of m_2 to the initial position, where k_2 is stretched, i.e., $m_2 g/k_2$.

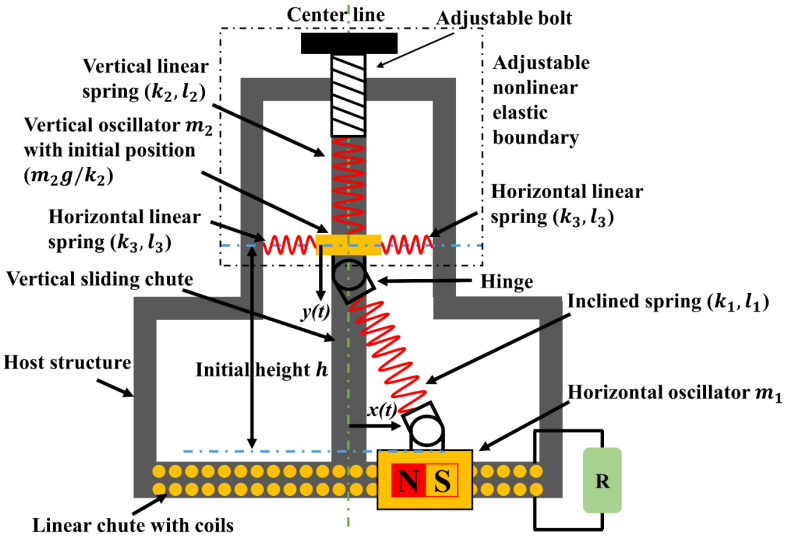

Fig. 1 Schematic diagram of the BEH-NB.

The kinetic energy of the BEH-NB is given as

$$T = \frac{1}{2}m_1(\dot{x} + \dot{z})^2 + \frac{1}{2}m_2(\dot{y} + \dot{z})^2 \tag{1}$$

where the operator $(\dot{})$ denotes the derivative to the time τ, $\ddot{z}$ is the base acceleration excitation given by $\ddot{z} = -A\cos(\Omega\tau)$ with Ω being the frequency of the excitations.

The potential energy of the BEH-NB is given as

$$U = \frac{1}{2}k_1\left(\sqrt{(h-y)^2 + x^2} - l_1\right)^2 + \frac{1}{2}k_2\left(\frac{m_2 g}{k_2} + y\right)^2 + k_3\left(\sqrt{y^2 + l_3^2} - l_3\right)^2 - m_2 g y \tag{2}$$

The dissipation function of the BEH-NB is given as

$$D = \frac{1}{2}c_1\dot{x}^2 + \frac{1}{2}c_2\dot{y}^2 \tag{3}$$

By applying the Euler-Lagrange principle and the Kirchhoff's law, the equations of BEH-NB subjected to the base acceleration excitation can be written as

$$m_1\ddot{x} + k_1 x\left(1 - \frac{l_1}{\sqrt{x^2 + (h-y)^2}}\right) + c_1\dot{x} = -m_1\ddot{z} - C_e c \tag{4a}$$

$$m_2\ddot{y} + k_2 y + 2k_3 y\left(1 - \frac{l_3}{\sqrt{l_3^2 + y^2}}\right) - k_1(h-y)\left(1 - \frac{l_1}{\sqrt{x^2 + (h-y)^2}}\right) + c_2\dot{y} = 0 \tag{4b}$$

$$L_e\dot{c} + Rc = C_e\dot{x} \tag{4c}$$

where c is the current flow through the resistance R. L_e is the inductance of the electromagnetic converter. C_e is the electromagnetic coupling constant.

To better facilitate the exploration of the original physical meaning of the equation,

introducing dimensionless variables and parameters: $X = x/l_1,\ Y = y/h,\ \omega_1 = \sqrt{k_1/m_1},\ \omega_2 = \sqrt{k_2/m_2},\ \omega_3 = \sqrt{k_3/m_2},\ \lambda = m_1/m_2,\ \mu_1 = k_1/k_2,\ \mu_2 = k_1/k_3,\ \eta_1 = h/l_1,\ \eta_2 = h/l_3,\ \varphi_1 = c_1/m_1\omega_1,\ \varphi_2 = c_2/m_2\omega_1,\ \omega = \Omega/\omega_1,\ t = \omega_1\tau,\ I = c/c_0,\ P = p/l_1\omega_1^2,\ \rho = C_e c_0/m_1 l_1 \omega_1^2,\ \theta = R/L_e\omega_1,\ \varepsilon = C_e l_1/L_e c_0.$

The dimensionless equations of BEH-NB are

$$\mathrm{X}'' + \mathrm{X}\left(1 - \frac{1}{\sqrt{X^2 + \eta_1^2(1-Y)^2}}\right) + \varphi_1 X' = \mathrm{P}\cos(\omega \mathrm{t}) - \rho \mathrm{I} \tag{5a}$$

$$\mathrm{Y}'' + \frac{\lambda}{\mu_1}Y + 2\frac{\lambda}{\mu_2}Y\left(1 - \frac{1}{\sqrt{1+\eta_2^2 Y^2}}\right) - \lambda(1-Y)\left(1 - \frac{1}{\sqrt{X^2 + \eta_1^2(1-Y)^2}}\right) + \varphi_2 Y' = 0 \tag{5b}$$

$$I' + \theta I = \varepsilon X' \tag{5c}$$

where the operator $()'$ is the derivative with respect to dimensionless time t.

3. Experiment validation of the model

3.1 Experimental setup

Before conducting an insightful investigation of the BEH-NB dynamics, the analytical model of BEH-NB should be validated. Therefore, the experiments are conducted to validate the dynamic response of the BEH-NB under the swept harmonic excitation in this section. The experimental prototype of the BEH-NB was manufactured as shown in Fig. 2(a-c) and the flowchart of the experimental procedure is shown in Fig. 2(d). The prototype is mounted on a shaker. The shaker can generate an excitation according to the designated signal input from the controller, which is used to excite the prototype. The swept harmonic acceleration excitation from 1 Hz to 10 Hz at a rate of 0.025 Hz/s is employed in this section. Two accelerometers are used to acquire the vibration acceleration of the horizontal oscillator m_1 and the shaker, respectively. The dynamic response of BEH-NB can be calculated from the acquired vibration acceleration data. The approximate values of the structural parameters of the prototype are presented in Table 1. It is worth noting that the damping constants c_1 and c_2 are estimated through parameter identification.

Table 1

Parameters of the experimental setup.

Parameter	Value
The horizontal oscillator m_1	0.684 kg
The vertical oscillator m_2	0.327 kg
The inclined spring stiffness k_1	1045 N/m
The vertical linear spring stiffness k_2	1020 N/m
The horizontal linear spring stiffness k_3	980 N/m
The inclined spring length l_1	0.08 m
The vertical linear spring length l_2	0.07 m
The horizontal linear spring length l_3	0.04 m
The initial height h	0.076 m
The damping constant c_1	1.9 Ns/m
The damping constant c_2	1.1 Ns/m

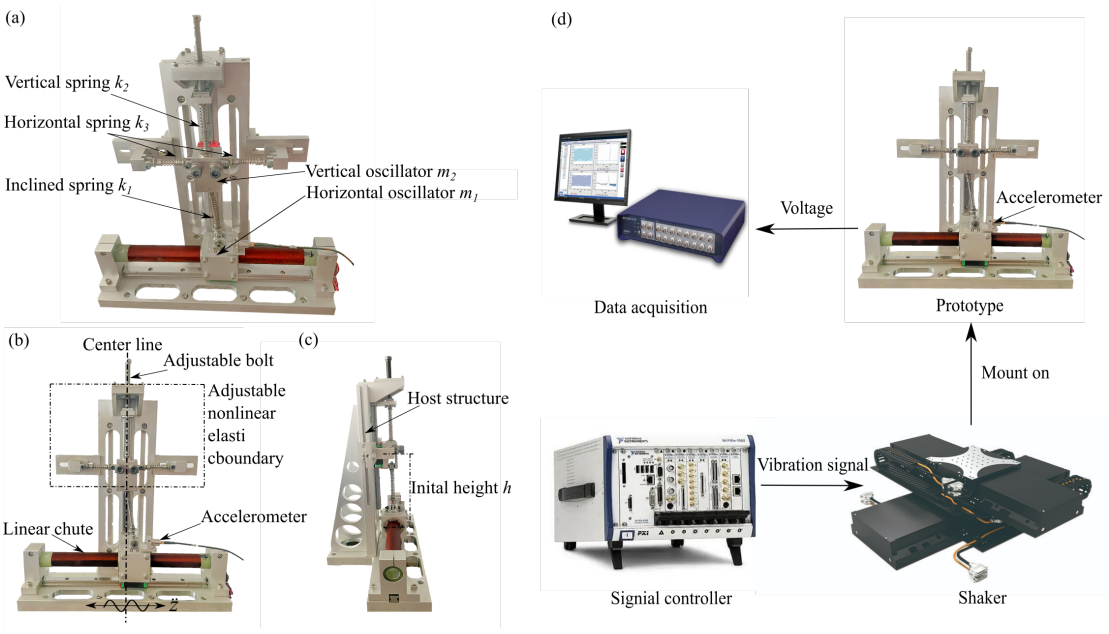

Fig. 2 The experimental prototype of BEH-NB: (a) aerial view; (b) front view; (c) lateral view; and (d) the flowchart of the experimental procedure.

3.1 Results

Figs. 3(a) and (c) show the experimental and numerical results of the acceleration envelope of the BEH-NB under the forward swept harmonic excitation with $A = [2.77, 3.37]$ m/s^2. Figs. 3(b) and (d) show the backward swept harmonic excitation with $A = [2.77, 3.37]$ m/s^2. From the comparison of the results, it can be found that the forward swept harmonic excitation can excite greater acceleration amplitude than backward swept harmonic excitation under the same excitation amplitude, which is similar to the phenomenon of the bistable system [35]. It can be

seen that the experimental results and the numerical results are in good agreement. A slight discrepancy is also spotted, which could be caused by the accuracy of the accelerometers and the measurement errors of the parameters. On the whole, the analytical model fidelity of the BEH-NB is verified by the experiments. This will guarantee the accuracy and reliability of the subsequent studies.

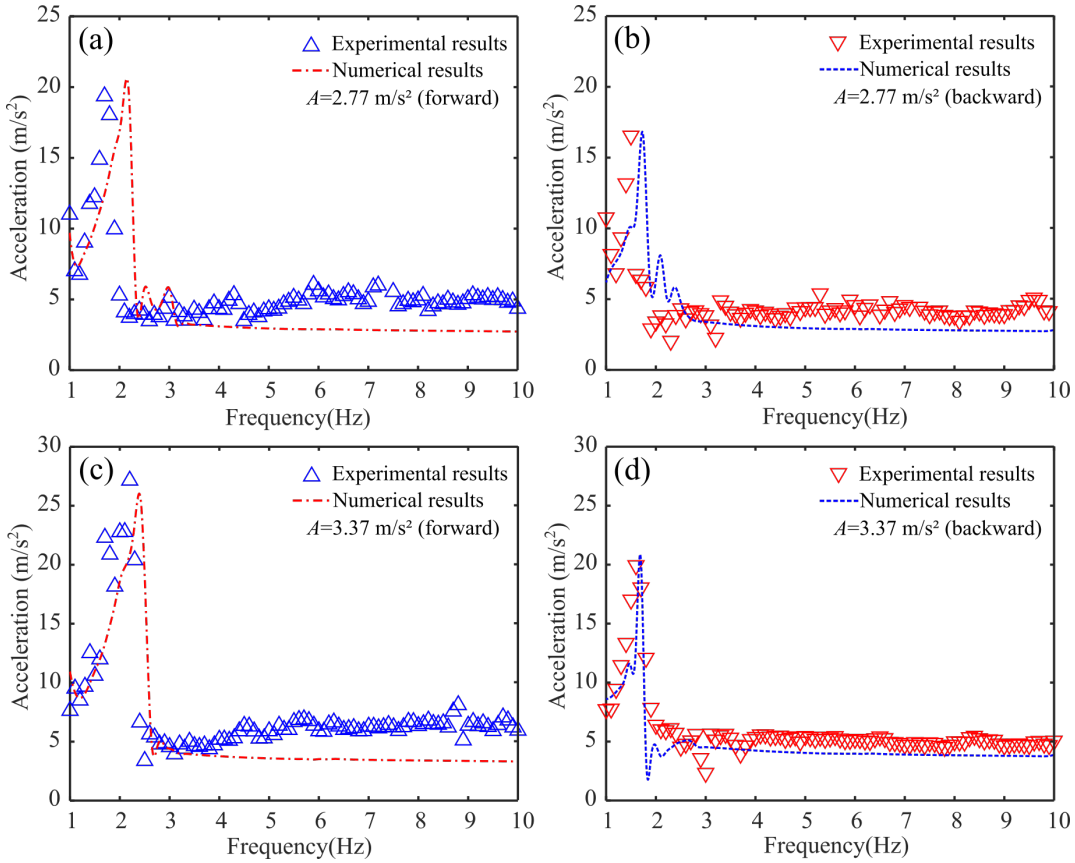

Fig. 3 The experimental and numerical results of the acceleration envelope of the BEH-NB subjected to (a)(c) the forward swept excitation with amplitude $A = 2.77\ \mathrm{m/s^2}$ and $\mathrm{A} = 3.37\ \mathrm{m/s^2}$, respectively; (b)(d) the backward swept excitation with amplitude $\mathrm{A} = 2.77\ \mathrm{m/s^2}$ and $A = 3.37\ \mathrm{m/s^2}$, respectively.

4. Performance comparison

To reveal the merits of the BEH-NB, the governing equations of the BEH-LB, the BEH, and a linear energy harvester (LEH) are established for comparison purpose. This section comparatively investigates the displacement and the velocity of the BEH-NB and its counterparts. In this way, it confirms whether the BEH-NB has potential research significance and application value. It also ensures that the subsequent studies are feasible and practically

meaningful.

4.1 Counterparts modeling

The governing equations of the BEH-LB are

$$m_1\ddot{x} + k_1 x\left(1 - \frac{l_1}{\sqrt{x^2 + (h-y)^2}}\right) + c_1\dot{x} = -m_1\ddot{z} - C_e c \tag{6a}$$

$$m_2\ddot{y} + k_2 y - k_1(h-y)\left(1 - \frac{l_1}{\sqrt{x^2 + (h-y)^2}}\right) + c_2\dot{y} = 0 \tag{6b}$$

$$L_e\dot{c} + Rc = C_e\dot{x} \tag{6c}$$

The governing equations of the BEH are

$$m_1\ddot{x} + k_1 x\left(1 - \frac{l_1}{\sqrt{x^2 + (h-y)^2}}\right) + c_1\dot{x} = -m_1\ddot{z} - C_e c \tag{7a}$$

$$F_n = k_1 x\left(1 - \frac{l_1}{\sqrt{x^2 + h^2}}\right) \tag{7b}$$

$$L_e\dot{c} + Rc = C_e\dot{x} \tag{7b}$$

where the F_n is the nonlinear restoring force.

The LEH is derived from the linearization of the BEH. When the BEH undergoes a small base acceleration excitation, the bistable nonlinearity of the BEH can be neglected, so that its response is almost identical to its linearized counterpart. Mass m_1 will oscillate around one of two stable equilibrium points. Its response can be expressed by $\Delta x = x - x_e$, where Δx is the new displacement variable with its origin at the equilibrium point x_e. The governing equation of the LEH can be expanded by using the Taylor series of the nonlinear restoring force F_n at equilibrium point and omitting the high order terms. The linear restoring force therewith be obtained as $F_l = k_1(1 - h^2/l_1^2)\Delta x$. Thus, the governing equations of the LEH are

$$m_1\ddot{\Delta x} + k_1\Delta x\left(1 - \frac{h^2}{l_1^2}\right) + c_1\dot{\Delta x} = -m_1\ddot{z} \tag{8a}$$

$$L_e\dot{c} + Rc = C_e\dot{\Delta x} \tag{8b}$$

4.2 Comparison results

A comparative study of the performance of the four types of energy harvesters is conducted. Numerical results are obtained based on the derived governing equations using the 4th order

Runge-Kutta algorithm. In the following simulations, the parameters are set as: $l_1 = 0.08$ m, $l_3 = 0.04$ m, $k_1 = 2000$ N/m, $k_2 = 2000$ N/m, $k_3 = 2000$ N/m, $m_1 = 0.2$ kg, $m_2 = 0.05$ kg, $c_1 = 0.1$ Ns/m, $c_2 = 0.1$ Ns/m, $h = 0.072$ m, $C_e = 0.8$ Tm, $R = 10\ \Omega$, $L_e = 0.005$ H. The equilibrium point is $x_e = \pm 0.0349$ m, $y_e = 0$ m. The initial conditions of the four types of energy harvesters are set at the stationary state, where the initial position of the LEH is $\Delta x = 0$m. The excitation used in this section is forward swept harmonic acceleration excitation in $0 - 10$ Hz at a rate of 0.025 Hz/s. The parameters used in the subsequent study remain the same unless otherwise stated. It is worth noting that for energy harvesters, a larger displacement and a larger velocity represent better performance. To make it clear, the power (i.e., $P(t) = c^2(t) * R$) is calculated, respectively.

Fig. 4 shows the displacement, velocity, and power for BEH-NB, BEH-LB, BEH, and LEH under swept harmonic acceleration excitation with amplitude $\mathrm{A} = 4\ \mathrm{m/s^2}$. It is clear that velocity and power are positively correlated. It can be seen that LEH can exhibit large oscillation only around the resonant frequency of 7 Hz. That means the operational bandwidth of LEH is very narrow and relatively small displacement and velocity can be achieve by LEH at frequencies away from the resonance. BEH can cross the potential energy barrier to produce inter-well oscillation (i.e., snap-through motion) only at the frequency of $5.8 - 6.1$ Hz, and the rest of the cases are intra-well oscillations. BEH-LB can complete inter-well oscillations only around 2.4 Hz and in the frequency of $3.8 - 6.8$ Hz. The rest of the cases are intra-well oscillations. Neither BEH nor BEH-LB can yield large velocities. BEH-NB obviously has a larger resonance region i.e., a larger operational bandwidth, and correspondingly a larger oscillation displacement and velocity. Only the BEH-NB behaves as an inter-well oscillation when the frequency exceeds 7.3 Hz, which is unique from the other three types of energy harvesters.

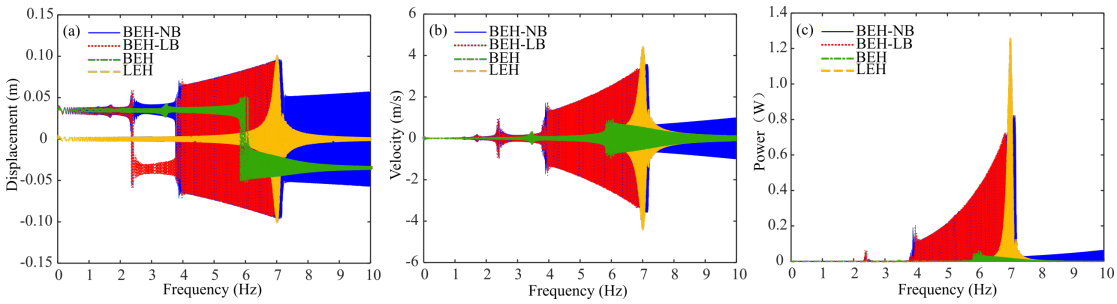

Fig. 4 (a) Displacement, (b) velocity, and (c) power for BEH-NB, BEH-LB, BEH, and LEH under swept harmonic acceleration excitation with amplitude $\mathrm{A} = 4\ \mathrm{m/s^2}$.

Fig. 5 shows the displacement, velocity, and power for BEH-NB, BEH-LB, BEH, and LEH under swept harmonic acceleration excitation with amplitude $\mathrm{A} = 6\ \mathrm{m/s^2}$. It can be seen that when the excitation amplitude increases, the displacement and the velocity of oscillation also increase. Specifically, the LEH can only grow linearly with the external input energy around the resonant frequency. This indicates that LEH has a narrow operational bandwidth and poor environmental adaptation and robustness in practical applications. The inter-well oscillation frequency of BEH increases from $5.8 - 6.1\ \mathrm{Hz}$ at $\mathrm{A} = 4\ \mathrm{m/s^2}$ to $5.4 - 6.3\ \mathrm{Hz}$ at $\mathrm{A} = 6\ \mathrm{m/s^2}$. BEH-LB and BEH-NB can cross the potential barrier at a lower frequency (i.e., 1.5 Hz) to achieve the inter-well oscillation. BEH-LB cannot sustainably cross the potential barrier and turns back to intra-well oscillation (i.e., $2.3 - 3.4\ \mathrm{Hz}$). The second resonance region is excited between $3.4 - 7\ \mathrm{Hz}$ to achieve the inter-well oscillation. The BEH-NB is able to maintain the inter-well oscillation after 1.5 Hz. It has a larger operational bandwidth and oscillation velocity. The comparison results show a large performance disparity between LEH and BEH compared to BEH-LB and BEH-NB. In other words, the additional coupled dynamical effect of the elastic boundary to the bistable energy harvester improves the performance of the system. Meanwhile, BEH-NB has better performance and robustness.

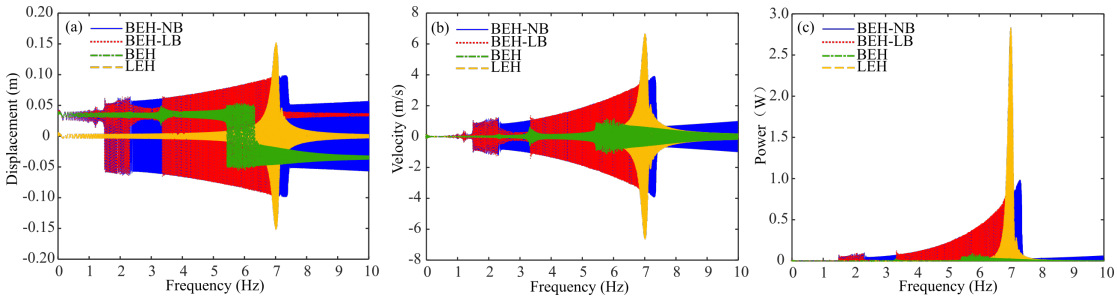

Fig. 5 (a) Displacement, (b) velocity, and (c) power for BEH-NB, BEH-LB, BEH, and LEH under swept harmonic acceleration excitation with amplitude $\mathrm{A} = 6\ \mathrm{m/s^2}$.

In order to gain a deeper understanding of the performance of the bistable energy harvester with different elastic boundaries, the maximum displacement and maximum velocity of BEH-NB and BEH-LB are tested under forward swept harmonic acceleration excitation with amplitude $\mathrm{A} = 0.5 - 10\ \mathrm{m/s^2}$. The average power (i.e., $\mathrm{E}[P(t)] = \mathrm{E}[c^2(t)] * R$) is also calculated, respectively. As shown in Fig. 6(a) and (b), when $\mathrm{A} < 1\ \mathrm{m/s^2}$, BEH-NB and BEH-

LB cannot cross the potential barrier and exhibit the intra-well oscillation. When $A > 1\ m/s^2$, both can achieve inter-well oscillation. From the other perspective, the maximum displacement and maximum velocity of both are basically the same when $A < 4\ m/s^2$, which indicates the performance of both is not much different. However, BEH-NB can achieve larger displacement and velocity than BEH-LB when $A \geq 4\ m/s^2$, leading to greater average power. It can be seen from Fig. 6(c) that the average power and the velocity have the same trend. This is consistent with the definition of dynamic electromotive force. Moreover, BEH-NB outperforms BEH-LB under the same excitation amplitude.

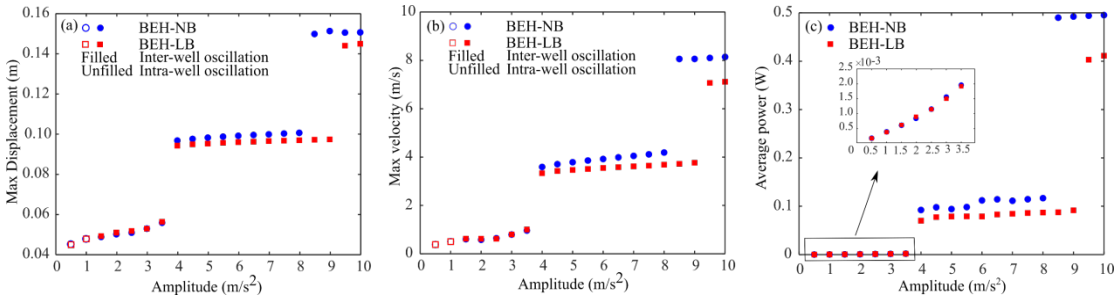

Fig. 6 Envelope of (a) displacement and (b) velocity and (c) average power for BEH-NB and BEH-LB under swept harmonic acceleration excitation with amplitude $A = 0.5 - 10\ m/s^2$, respectively.

From the above analysis, it can be seen that the operational bandwidth of LEH is narrow, which indicates that the LEH can only be effective near its intrinsic frequency. Furthermore, the system performance decreases sharply when the excitation frequency deviates from the intrinsic frequency. The bistable nonlinearity brings BEH, BEH-LB, and BEH-NB wider operational bandwidths and improves the performance of the system. With a lower snap-through threshold, the elastic boundary can further enhance the harvest performance. However, BEH-NB can achieve a larger amplitude inter-well oscillation with the same excitation amplitude. Meanwhile, better performance and robustness of the system can be achieved. Overall, due to the bistable nonlinearity, the bistable energy harvesters have a larger operational bandwidth. The coupling elastic boundary brings an additional dynamic coupling effect to the bistable energy harvester further improving the output performance, while the nonlinear elastic boundary enables the bistable energy harvester to perform better than the one with linear elastic boundary. This high-performing BEH-NB, therefore, has a more widespread application scenario.

5. Bifurcation analyses

The bifurcation indicates a qualitative change in a system behavior due to an infinitesimally small change in bifurcation parameter, whether internal or external to the system. Therefore, it is necessary to perform bifurcation analyses to understand the nonlinear vibration characteristics of the BEH-NB. This section investigates the bifurcation of the BEH-NB in terms of inclined spring stiffness k_1, horizontal oscillator m_1, stiffness ratio μ_1, and mass ratio λ. The excitation parameters are set as $A = 6\ \mathrm{m/s^2}$ and $\Omega = 5\ \mathrm{Hz}$. The initial conditions of the oscillator are set at one of the static equilibrium points (i.e., $[x_e, y_e, \dot{x}, \dot{y}] = [0.0349, 0, 0, 0]$). Phase diagrams and Poincaré sections are employed to reveal more clearly the effect of the above parameter variations on the nonlinear dynamic response. Poincaré section is the plot formed by the intersection of the motion trajectory and the plane set by the motion period. The black dots in the following figures denote Poincaré section. In the meantime, the effect of the initial conditions of BEH-NB on the steady-state response is investigated. The two sets of the initial conditions are selected. The first one is kept consistent with the initial conditions of the bifurcation diagram, which are static initial conditions. The other one is set to random initial conditions, that is, the position and the velocity of oscillators are randomly picked. Here, one thing that should be noted is that the stroboscopic time $1/\Omega$ for the excited system is adopted in both the bifurcation diagrams, phase diagrams, and Poincaré sections.

5.1 Bifurcation characteristics of the structural parameters

Fig. 7(a) shows the bifurcation diagram of BEH-NB with respect to inclined spring stiffness k_1 versus the horizontal oscillator m_1 displacement x. The k_1 ranges from $50 - 30000\ \mathrm{N/m}$ in steps of $10\ \mathrm{N/m}$. It can be seen that k_1 plays a decisive role in the steady-state response of BEH-NB, which contributes directly to the efficiency of energy harvesting. As the results of the bifurcation diagram, an excessively small k_1 prevents m_1 crossing the potential barrier, but helps to maintain the intra-well oscillation. With the gradual increase of k_1, the steady-state response starts to bifurcate and exhibits more abundant nonlinear dynamic phenomena like chaos. Later on, the system bifurcates into intra-well oscillation when $698\ \mathrm{N/m} < k_1 < 1166\ \mathrm{N/m}$. As k_1 exceeds $1168\ \mathrm{N/m}$, the response bifurcates into

chaotic inter-well oscillation again. The phase diagrams and Poincaré sections at the initial conditions of the stationary state and random state are presented in Figs. 7(b)-(g). It can be observed that the initial conditions have a crucial influence on the steady-state response, displacement amplitude, and velocity. Figs. 7(b-d) demonstrate a suitable k_1 can amplify the displacement amplitude and velocity, which will significantly improve the energy harvesting performance. The random initial conditions therewith are selected as shown in Figs. 7(e-g). The BEH-NB presents a completely distinct steady-state response from that in which the static initial conditions are selected. It leads to larger displacement and velocity than those at static initial conditions in Figs. 7(b-d).

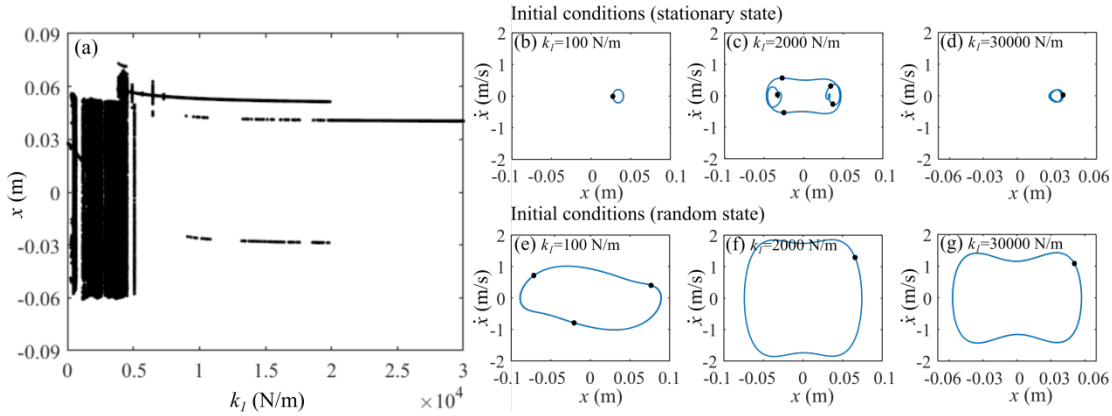

Fig. 7 (a) Bifurcation diagram of the inclined spring stiffness k_1 versus the displacement x. (b-g) Phase diagrams and Poincaré sections under different k_1 and different initial conditions.

The bifurcation diagram of BEH-NB with respect to the horizontal oscillator m_1 versus the horizontal oscillator m_1 displacement x is shown in Fig. 8(a). $m_1 = 0.01 - 5$ kg with an interval of 0.01 kg. Similarly, it can be seen that a too small value of m_1 will result in the BEH-NB only producing inefficient intra-well oscillation as shown in Fig. 8(b). According to the law of kinetic energy, it is known that when m_1 is small enough, this means that the kinetic energy stored by m_1 is also small, so this will lead to m_1 not reaching the potential energy threshold to achieve favorable large amplitude inter-well oscillation. With the increase of m_1, BEH-NB goes through intra-well oscillations, chaotic inter-well oscillations, periodic inter-well oscillations, and finally bifurcates into quasi-periodic intra-well oscillations. It is evident that the selection of a suitable m_1 value is beneficial to excite efficient inter-well oscillation. For example, comparing Figs. 8(c) and (f), the BEH-NB achieves chaotic inter-well oscillation under static initial conditions. By changing to the random initial conditions, it exhibits

completely different nonlinear dynamical phenomena from static initial conditions. BEH-NB achieves periodic inter-well oscillation, which manifests a greater displacement amplitude and velocity. A similar phenomenon occurs when $m_1 = 1$ kg in Figs. 8(d) and (g), where BEH-NB is excited at the static initial conditions to produce quasi intra-well oscillation into a quasi-periodic inter-well oscillation when excited in the random initial conditions. However, Figs. 8(b) and (e) shows that changes in the initial conditions may not necessarily change the type of response either.

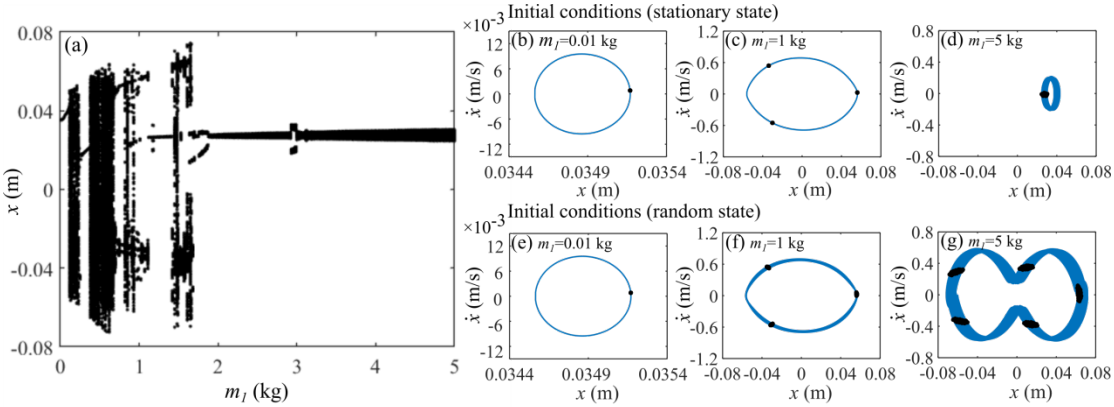

Fig. 8 (a) Bifurcation diagram of the horizontal oscillator m_1 versus the displacement x. (b-g) Phase diagrams and Poincaré sections under different m_1 and different initial conditions.

Dimensionless parameters study is also crucial. Fig. 9(a) shows the bifurcation diagram of BEH-NB with respect to the stiffness ratio μ_1 versus the dimensionless displacement X. The μ_1 ranges from $0.1 - 15$ in steps of 0.02. To illustrate more prominently, Figs. 9(b)-(g) show three representative sets of stiffness ratio's Phase diagrams and Poincaré sections. It is seen that when $\mu_1 = 0.1$, the BEH-NB is only able to do intra-well oscillation near either of two equilibrium points. Then as μ_1 increases, the BEH-NB can overcome the potential barrier to the inter-well oscillations. At the same time, the displacement amplitude and the velocity are also increasing. This represents better energy harvesting performance. However, as μ_1 continues to increase, for example $\mu_1 = 15$, the displacement amplitude and the velocity are reduced by an order of magnitude. Therefore, it can be found that μ_1 has a certain range that is favorable for performance. Exceeding this range or being less than this range will lead to the degradation of the performance.

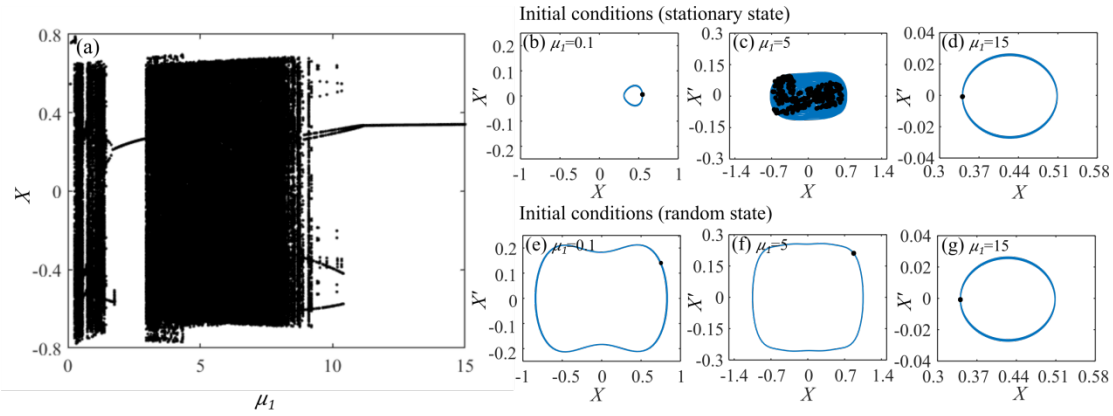

Fig. 9 (a) Bifurcation diagram of the stiffness ratio μ_1 versus the dimensionless displacement X. (b-g) Phase diagrams and Poincaré sections under different μ_1 and different initial conditions.

The bifurcation diagram of BEH-NB with respect to the mass ratio λ versus the dimensionless displacement X is shown in Fig. 10(a). $\lambda = 0.01 - 15$ with an interval of 0.02. It is obvious to see that chaotic inter-well oscillation is the dominant steady-state response of the system. This seems to indicates that the susceptibility of the steady-state response to mass ratio is comparatively low. With delve into λ in more detail, it was found that the system performance is poorer when λ is relatively small, as shown in Figs. 10(b)-(g). Hence, in order to obtain a higher energy harvesting efficiency, particularly small λ should be avoided. More attention can be paid to the selection of the appropriate m_1 during the structural design.

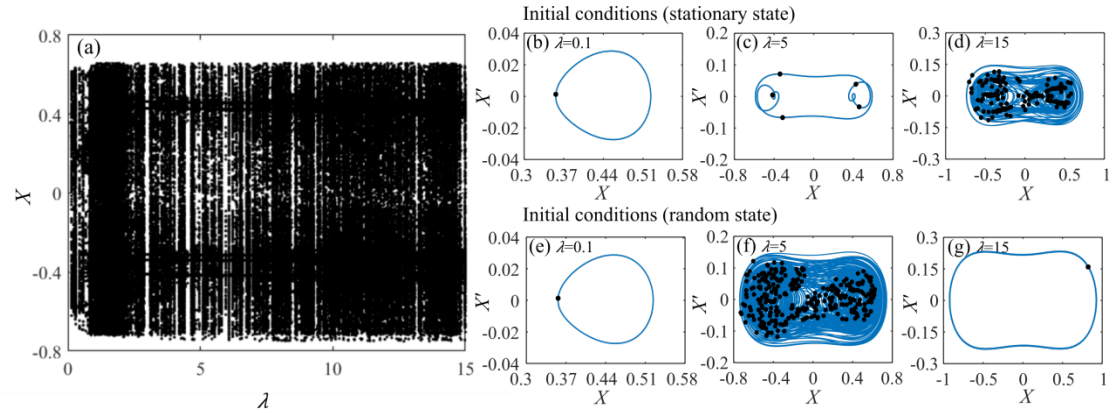

Fig. 10 (a) Bifurcation diagram of the mass ratio λ versus the dimensionless displacement X. (b-g) Phase diagrams and Poincaré sections under different λ and different initial conditions.

5.2 Bifurcation characteristics of the excitation parameters

Besides the structural parameters, different excitation parameters will profoundly influence the steady-state response of BEH-NB. Therefore, this section is devoted to discussing the fundamental excitation parameters in terms of excitation frequency Ω and excitation

amplitude A on the bifurcation characteristics of the system.

In Fig. 11(a), the bifurcation diagram of BEH-NB with respect to excitation frequency Ω versus the horizontal oscillator m_1 displacement x is shown, for $\Omega = 0.1 - 10$ Hz with the step of 0.01 Hz. The two resonant regions of BEH-NB can be seen in Fig. 11(a). As Ω increases, the steady-state response of the system undergoes intra-well oscillation, chaotic inter-well oscillations, and periodic inter-well oscillations. Figs. 11(b)-(g) show three representative results. As can be seen in Figs. 11(c) and (f), different initial conditions may change the steady-state response of the system. For instance, the dynamic response can change from inefficient small-amplitude intra-well oscillation at static initial conditions to efficient large-amplitude inter-well oscillation at random initial conditions when $\Omega = 6$ Hz. However, when $\Omega = 10$ Hz, the response of the system remains unchanged when the initial conditions are changed. This means that it is difficult to excite the inter-well oscillation far from the resonant frequency. Sometimes changing the initial conditions does not affect the steady-state response, which reflects the stochastic dependence and uncertainty of the nonlinear system on the initial conditions. There are some interesting phenomena shown in Figs. 11(b), (e), and (f), called chaos in dissipative systems, where two strange attractors are clearly distinguished in the phase diagram. This phenomenon is not existing in the conservative system. The m_1 will move randomly in a chaotic manner around the two strange attractors but within a clear boundary. In general, the BEH-NB is more likely to resonate near its eigenfrequency, producing efficient inter-well oscillation. It is difficult to realize inter-well oscillation and the performance of BEH-NB is extremely curtailed when Ω is far from the characteristic frequency of the system. Therefore, in practical application, the system parameters should be modified according to the application scenario so that the eigenfrequency is close to the ambient frequency. This will greatly boost the performance of the energy harvester.

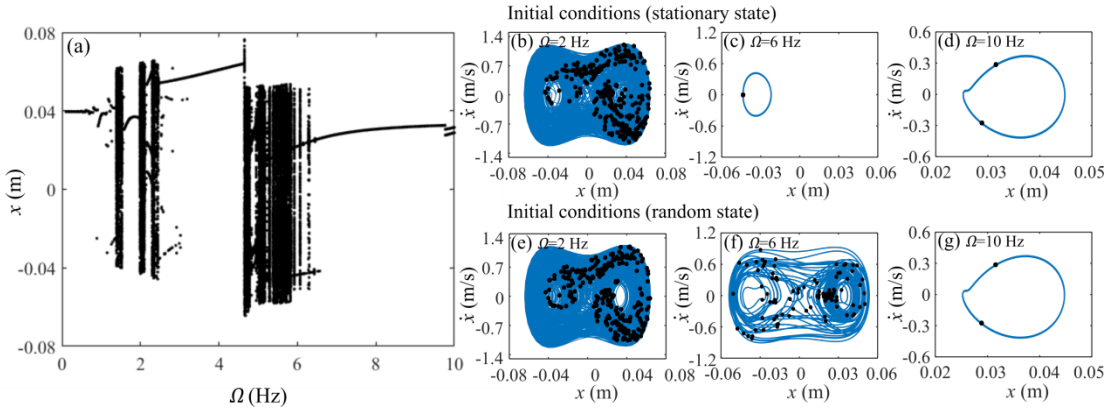

Fig. 11 (a) Bifurcation diagram of the excitation frequency Ω versus the displacement x. (b-g) Phase diagrams and Poincaré sections under different Ω and different initial conditions.

Fig. 12(a) is a bifurcation diagram of BEH-NB with respect to the excitation amplitude A versus the displacement x. The range of A is $0.1-10\ \mathrm{m/s^2}$ in steps of $0.1\ \mathrm{m/s^2}$. When A is small, the energy obtained by m_1 is less than the threshold value, which is insufficient for BEH-NB to overcome the potential barrier. The system therewith exhibits a small amplitude intra-well motion. As A increases, the external input energy increases and the steady-state response begins to behave as chaotic inter-well oscillation. When A is further increased, the steady-state response changes to a stable large-amplitude periodic inter-well oscillation, which means higher efficiency of energy harvesting. Two strange attractors are also observed in Fig. 12(c), where the steady-state response can change to a larger amplitude periodic inter-well oscillation when the initial conditions changes to random initial conditions, as shown in Fig. 12(f). In general, too small A prevents the BEH-NB from exciting inter-well oscillation. As A increases, the system is more likely to overcome the potential barrier to achieving inter-well oscillation, which also amplifies the energy harvesting efficiency. However, the system reaches saturation and the energy harvesting efficiency does not increase further when A reaches a certain value.

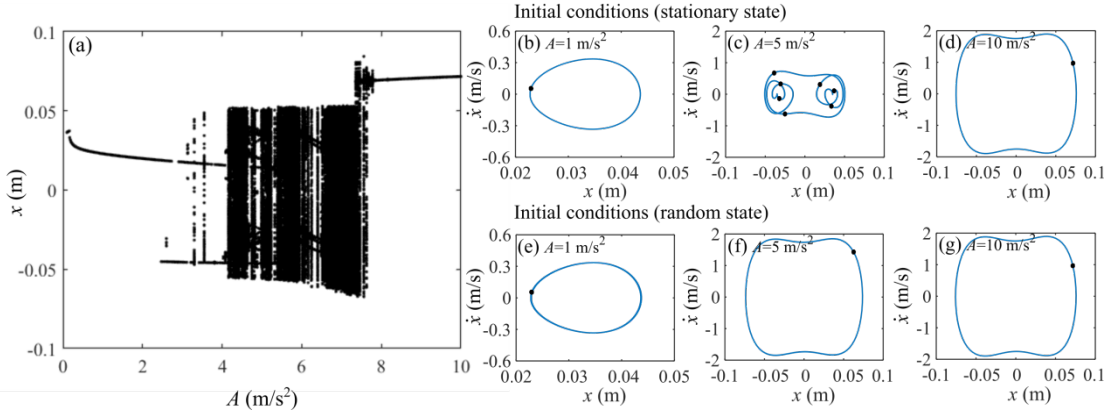

Fig. 12 (a) Bifurcation diagram of the excitation amplitude A versus the displacement x. (b-g) Phase diagrams and Poincaré sections under different A and different initial conditions.

6. Basin of attraction

The above study found that the dynamics of the system can be sensitively dependent on the initial conditions. Once the parameters of the system are kept constant, the initial conditions become the most important factor in determining the steady-state response of the system and the performance of energy harvesting. Therefore, this section focused on the basin of attraction of BEH-NB. The basins of attraction are computed to investigate the steady-state dynamic behavior of the system under a set of given initial conditions. Multiple excitation frequencies $\Omega = [1,10]$ Hz with the step of 1 Hz are selected, and the range is set to $[-0.06,0.06]$ m $\times$ $[-1,1]$ m/s, including 201×201 equidistantly different initial conditions. When m_1 is excited from these different initial conditions, it will eventually generate intra-well oscillation, periodic inter-well oscillation, and chaotic inter-well oscillation, respectively. In the basins of attraction in this section, blue, red, and yellow represent intra-well oscillation, periodic inter-well oscillation, and chaotic inter-well oscillation, respectively. The width of the wells indicated by black lines to make it easier to see if the different steady-state response are lies on or close to these boundaries. It is worth noting that snap-through motions come with high energy harvesting efficiency regardless of the type of inter-well oscillations.

6.1 Sensitivity study of BEH-NB to initial conditions

Fig. 13 shows the basins of attraction of the BEH-NB at the excitation amplitude $A = 3$ m/s^2. It can be seen that the blue "teardrop" appeared around the strange attractor, which means that the steady-state response from the static equilibrium position and small velocity is excited with a high probability of intra-well oscillation. As the frequency increases from 1 Hz to 4 Hz, the system gradually changes from a large probability of intra-well oscillation to chaotic inter-well oscillation. The probability of snap-through motions spiking to a maximum when $\Omega = 4$ Hz. As the frequency continues to increase, the probability of inter-well oscillation decreases and then increases. The yellow "striped" region can be seen at $\Omega = 7 - 9$ Hz, indicating that the steady-state response of the system is more likely to become chaotic inter-well oscillation at larger initial velocities. This is because the fact that the initial kinetic

energy of the system can cross the potential barrier, while the smaller initial velocity makes the initial kinetic energy of the system insufficient to sustainably break through the potential barrier, i.e., it is possible to be excited with inter-well response under suitable initial conditions. When $\Omega = 10$ Hz, the steady-state response is almost covered by the blue, at which frequency the probability of snap-through motion is rare and the intra-well motion is once again the dominant dynamic response.

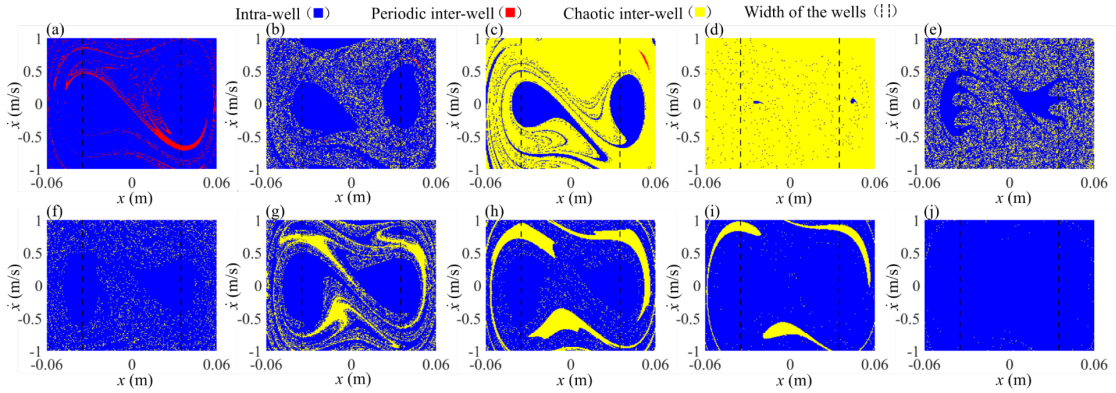

Fig. 13 Basins of attraction of BEH-NB at $A = 3\ \mathrm{m/s^2}$. (a) $\Omega = 1$ Hz; (b) $\Omega = 2$ Hz; (c) $\Omega = 3$ Hz; (d) $\Omega = 4$ Hz; (e) $\Omega = 5$ Hz; (f) $\Omega = 6$ Hz; (g) $\Omega = 7$ Hz; (h) $\Omega = 8$ Hz; (i) $\Omega = 9$ Hz; (j) $\Omega = 10$ Hz;

The basin of attraction map of BEH-NB at the excitation amplitude $\mathrm{A} = 6\ \mathrm{m/s^2}$ is illustrated in Fig. 14. Comparison with Fig. 13 shows that the chaotic inter-well oscillation represented in yellow occupies more frequencies on the basin of attraction map. The probability of the snap-through motion is 100% at $\Omega = 2{,}4{,}5$ Hz. These are the resonant frequencies of the system. The probability of the snap-through motion of the system excited by this frequency is increased considerably, which is also the optimal operational frequency for BEH-NB. As the excitation frequency changes to higher frequencies, the system begins to be dominated by blue "droplets" near the strange attractor again, i.e., the steady-state response exhibits a small amplitude intra-well oscillation. Only with larger initial velocities can the potential barrier be crossed to realize efficient snap-through motion. In other words, the resonant frequency of the system should be ensured to be adjacent to the ambient excitation frequency. In a nutshell, there are two ways to enhance energy harvesting performance. On the one hand, the system parameters can be designed according to different application scenarios, so that the resonant frequency of the system can be matched with the ambient excitation frequency. On the other hand, giving the system a more favorable initial condition at the beginning. This will excite the

large amplitude snap-through motion to enhance the energy harvesting performance.

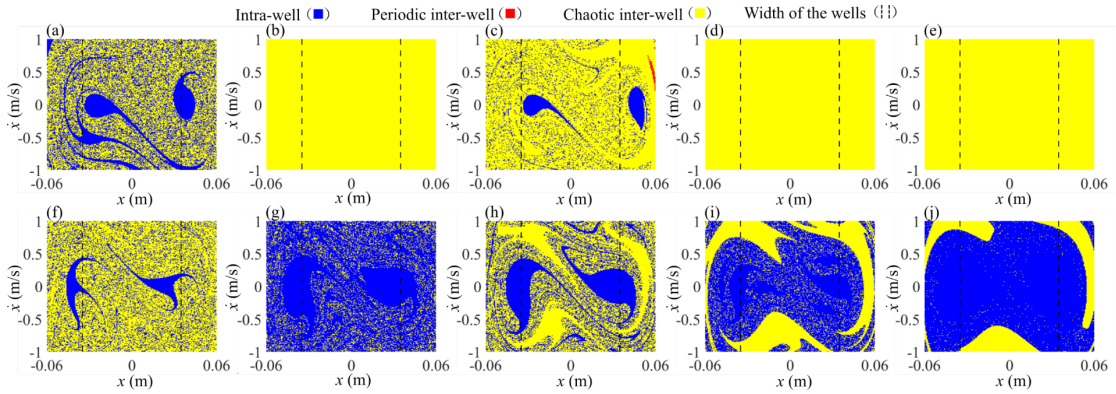

Fig. 14 Basins of attraction of BEH-NB at $A = 6\ \mathrm{m/s^2}$. (a) $\Omega = 1$ Hz; (b) $\Omega = 2$ Hz; (c) $\Omega = 3$ Hz; (d) $\Omega = 4$ Hz; (e) $\Omega = 5$ Hz; (f) $\Omega = 6$ Hz; (g) $\Omega = 7$ Hz; (h) $\Omega = 8$ Hz; (i) $\Omega = 9$ Hz; (j) $\Omega = 10$ Hz;

6.2 Occurrence probability of different dynamic behaviors

The basins of attraction can provide an intuitive qualitative result for the different initial conditions of BEH-NB. It is necessary to quantitatively analyze the occurrence probability of the dynamical response of BEH-NB in each frequency domain to reveal the role of initial conditions more clearly and specifically. Therefore, the occurrence probabilities of different dynamic behaviors are investigated for $\Omega = 1 - 10$ Hz, respectively.

The occurrence probabilities of different dynamic behaviors of BEH-NB at the excitation amplitude $\mathrm{A} = 3\ \mathrm{m/s^2}$ and $\mathrm{A} = 6\ \mathrm{m/s^2}$ are given in Figs. 15(a) and (b), respectively. It can be intuitively found that the probability of snap-through motion is significantly higher when $\mathrm{A} = 6\ \mathrm{m/s^2}$. This means that a larger excitation amplitude can enhance the performance of BEH-NB. With the increase of excitation amplitude, the snap-through motion has the same trend at different excitation frequencies. It is evident that the optimal operating frequency of the system is $\Omega = 4$ Hz, which can exhibit a snap-through motion probability close to 100% at both frequency amplitudes. It can also be found that BEH-NB performs better at low frequencies where the snap-through motion dominates the dynamic behaviors. The intra-well oscillation gradually dominates the dynamic behavior as the frequency increases. In particular, for small excitation amplitudes, the probability of efficient snap-through motion decreases rapidly when $\Omega \geq 5$ Hz. Increasing the external excitation amplitude can effectively boost the energy harvesting performance.

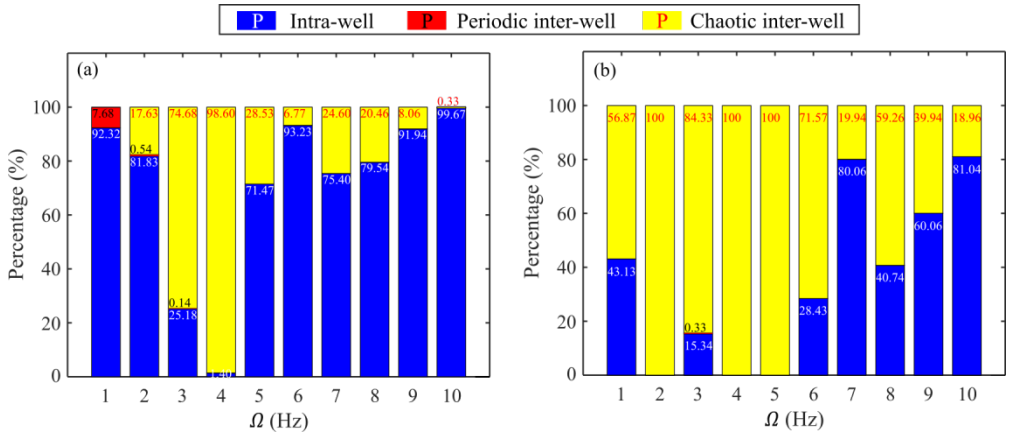

Fig. 15 Probability of different dynamic behaviors of BEH-NB at (a) $A = 3\ \mathrm{m/s^2}$, (b) $A = 6\ \mathrm{m/s^2}$.

7. Conclusions

This paper comprehensively investigates a novel bistable energy harvester coupled with a nonlinear elastic boundary. The BEH-NB is modeled and experimentally verified. To validate the advantages of the BEH-NB, the study performs the comparison of the BEH-NB, BEH-LB, BEH, and LEH. Results comparison shows that the BEH-NB has a broader operational bandwidth and better energy harvesting performance. The bifurcation analyses in terms of inclined spring stiffness k_1, horizontal oscillator mass m_1, stiffness ratio μ_1, mass ratio λ, excitation frequency Ω, and excitation amplitude A are presented to reveal the characteristic of BEH-NB. Furthermore, the basin of attraction and occurrence probability of BEH-NB are explored to mutually reveal the influence of the initial condition and resonant frequency of the system, which will guide practical application. It was found that higher external excitation amplitude resulting in higher input energy, can effectively boost the energy harvesting performance of the harvester. The results also indicate that the resonant frequency of the system should be contiguous with the ambient excitation frequency. This can be achieved by designing the system parameters according to different application scenarios.

Declaration of Competing Interest

The authors declare that they have no known competing financial interests or personal relationships that could have appeared to influence the work reported in this paper.

Acknowledgments

This work is supported by the National Natural Science Foundation of China (Grant No. 11802097) and the Young Topnotch Cultivation Program of Hubei Province.

References

[1] Mateu Loreto, and Moll Francesc. (2005). Review of energy harvesting techniques and applications for microelectronics. Paper presented at the VLSI Circuits and Systems II.

[2] Wei Chongfeng, and Jing Xingjian. (2017). A comprehensive review on vibration energy harvesting: Modelling and realization. Renewable and Sustainable Energy Reviews, 74, 1-18.

[3] Wang Junlei, Geng Linfeng, Ding Lin, Zhu Hongjun, and Yurchenko Daniil. (2020). The state-of-the-art review on energy harvesting from flow-induced vibrations. Applied Energy, 267, 114902.

[4] Wang Suo, Miao Gang, Zhou Shengxi, Yang Zhichun, and Yurchenko Daniil. (2022). A novel electromagnetic energy harvester based on the bending of the sole. Applied Energy, 314, 119000.

[5] Foong Faruq Muhammad, Thein Chung Ket, and Yurchenko Daniil. (2021). A novel high-power density, low-frequency electromagnetic vibration energy harvester based on anti-phase motion. Energy Conversion and Management, 238, 114175.

[6] Yang Tao, Zhang YongQi, and Zhou ShengXi. (2022). Multistage oscillators for ultra-low frequency vibration isolation and energy harvesting. Science China Technological Sciences, 65(3), 631-645.

[7] Munaz Ahmed, Lee Byung-Chul, and Chung Gwiy-Sang. (2013). A study of an electromagnetic energy harvester using multi-pole magnet. Sensors and Actuators A: Physical, 201, 134-140.

[8] Yurchenko Daniil, Machado Lucas Queiroz, Wang Junlei, Bowen Chris, Sharkh Suleiman, Moshrefi-Torbati Mohamed, and Val Dimitri V. (2022). Global optimisation approach for designing high-efficiency piezoelectric beam-based energy harvesting devices. Nano Energy, 93, 106684.

[9] Park Choon-Su, Shin Yong Chang, Jo Soo-Ho, Yoon Heonjun, Choi Wonjae, Youn Byeng D, and Kim Miso. (2019). Two-dimensional octagonal phononic crystals for highly dense piezoelectric energy harvesting. Nano Energy, 57, 327-337.

[10] Yang Tao, and Cao Qingjie. (2019). Dynamics and energy generation of a hybrid energy harvester under colored noise excitations. Mechanical Systems and Signal Processing, 121, 745-766.

[11] Zhang Yulong, Wang Tianyang, Luo Anxin, Hu Yushen, Li Xinxin, and Wang Fei. (2018). Micro electrostatic energy harvester with both broad bandwidth and high normalized power density. Applied Energy, 212, 362-371.

[12] Zou Hongxiang, Li Meng, Zhao Linchuan, Liao Xinwen, Gao Qiuhua, Yan Ge, Du Ronghua, Wei Kexiang, and Zhang Wenming. (2022). Cooperative compliant traction mechanism for human-friendly biomechanical energy harvesting. Energy Conversion and Management, 258, 115523.

[13] Wang Wei, Cao Junyi, Zhang Nan, Lin Jing, and Liao Wei-Hsin. (2017). Magnetic-spring based energy harvesting from human motions: Design, modeling and experiments. Energy Conversion and Management, 132, 189-197.

[14] Harne Ryan L, and Wang KW. (2013). A review of the recent research on vibration energy harvesting via bistable systems. Smart Materials and Structures, 22(2), 023001.

[15] Vocca Helios, Neri Igor, Travasso Flavio, and Gammaitoni Luca. (2012). Kinetic

energy harvesting with bistable oscillators. Applied Energy, 97, 771-776.
[16] Zhou Shengxi, Cao Junyi, Wang Wei, Liu Shengsheng, and Lin Jing. (2015). Modeling and experimental verification of doubly nonlinear magnet-coupled piezoelectric energy harvesting from ambient vibration. Smart Materials and Structures, 24(5), 055008.
[17] Hou Zehao, Zha Wenyu, Wang Hongbo, Liao Wei-Hsin, Bowen Chris R, and Cao Junyi. (2022). Bistable energy harvesting backpack: Design, modeling, and experiments. Energy Conversion and Management, 259, 115441.
[18] Li Xuefeng, Zhang Jingyu, Li Renfu, Dai Lu, Wang Wei, and Yang Kai. (2021). Dynamic responses of a two-degree-of-freedom bistable electromagnetic energy harvester under filtered band-limited stochastic excitation. Journal of Sound and Vibration, 511, 116334.
[19] Lan Chunbo, and Qin Weiyang. (2017). Enhancing ability of harvesting energy from random vibration by decreasing the potential barrier of bistable harvester. Mechanical Systems and Signal Processing, 85, 71-81.
[20] Yu Ning, Wu Chuanyu, Yu Gaohong, and Yan Bo. (2022). Bistable Electromagnetic Energy Harvesting Enhanced with a Resonant Circuit. In Advances in Nonlinear Dynamics (pp. 221-231): Springer.
[21] Jin Yanfei, and Zhang Yanxia. (2021). Dynamics of a delayed Duffing-type energy harvester under narrow-band random excitation. Acta Mechanica, 232(3), 1045-1060.
[22] Zhou Shengxi, and Zuo Lei. (2018). Nonlinear dynamic analysis of asymmetric tristable energy harvesters for enhanced energy harvesting. Communications in Nonlinear Science and Numerical Simulation, 61, 271-284.
[23] Sun Shuailing, Leng Yonggang, Su Xukun, Zhang Yuyang, Chen Xiaoyu, and Xu Junjie. (2021). Performance of a novel dual-magnet tri-stable piezoelectric energy harvester subjected to random excitation. Energy Conversion and Management, 239, 114246.
[24] Oumbé Tékam GT, Kitio Kwuimy CA, and Woafo P. (2015). Analysis of tristable energy harvesting system having fractional order viscoelastic material. Chaos: An Interdisciplinary Journal of Nonlinear Science, 25(1), 013112.
[25] Yan Bo, Zhou Shengxi, and Litak Grzegorz. (2018). Nonlinear analysis of the tristable energy harvester with a resonant circuit for performance enhancement. International Journal of Bifurcation and Chaos, 28(07), 1850092.
[26] Zhang Yanxia, and Jin Yanfei. (2021). Colored Lévy Noise-Induced Stochastic Dynamics in a Tri-Stable Hybrid Energy Harvester. Journal of Computational and Nonlinear Dynamics, 16(4).
[27] Zhou Zhiyong, Qin Weiyang, and Zhu Pei. (2017). A broadband quad-stable energy harvester and its advantages over bi-stable harvester: simulation and experiment verification. Mechanical Systems and Signal Processing, 84, 158-168.
[28] Zou Donglin, Chen Keyu, Rao Zhushi, Cao Junyi, and Liao Wei-Hsin. (2022). Design of a quad-stable piezoelectric energy harvester capable of programming the coordinates of equilibrium points. Nonlinear Dynamics, 1-15.
[29] Wang Qiang, Zhou Jiaxi, Xu Daolin, and Ouyang Huajiang. (2020). Design and experimental investigation of ultra-low frequency vibration isolation during neonatal transport. Mechanical Systems and Signal Processing, 139, 106633.
[30] Zhou Jiaxi, Xiao Qingyu, Xu Daolin, Ouyang Huajiang, and Li Yingli. (2017). A novel

quasi-zero-stiffness strut and its applications in six-degree-of-freedom vibration isolation platform. Journal of Sound and Vibration, 394, 59-74.

[31] Zhou Jiaxi, Wang Xinlong, Xu Daolin, and Bishop Steve. (2015). Nonlinear dynamic characteristics of a quasi-zero stiffness vibration isolator with cam–roller–spring mechanisms. Journal of Sound and Vibration, 346, 53-69.

[32] Yang Kai, Tong Weihao, Lin Liquan, Yurchenko Daniil, and Wang Junlei. (2022). Active vibration isolation performance of the bistable nonlinear electromagnetic actuator with the elastic boundary. Journal of Sound and Vibration, 520, 116588.

[33] Zou Donglin, Liu Gaoyu, Rao Zhushi, Tan Ting, Zhang Wenming, and Liao Wei-Hsin. (2021). A device capable of customizing nonlinear forces for vibration energy harvesting, vibration isolation, and nonlinear energy sink. Mechanical Systems and Signal Processing, 147, 107101.

[34] Lu Ze-Qi, Liu Wen-Hang, Ding Hu, and Chen Li-Qun. (2022). Energy Transfer of an Axially Loaded Beam With a Parallel-Coupled Nonlinear Vibration Isolator. Journal of Vibration and Acoustics, 144(5), 051009.

[35] Fang Shitong, Zhou Shengxi, Yurchenko Daniil, Yang Tao, and Liao Wei-Hsin. (2022). Multistability phenomenon in signal processing, energy harvesting, composite structures, and metamaterials: A review. Mechanical Systems and Signal Processing, 166, 108419.

[36] Zhang Yanxia, Duan Jinqiao, Jin Yanfei, and Li Yang. (2021). Discovering governing equation from data for multi-stable energy harvester under white noise. Nonlinear Dynamics, 106(4), 2829-2840.

[37] Yang Tao, and Cao Qingjie. (2020). Dynamics and high-efficiency of a novel multi-stable energy harvesting system. Chaos, Solitons & Fractals, 131, 109516.

[38] Harne RL, Thota M, and Wang KW. (2013). Bistable energy harvesting enhancement with an auxiliary linear oscillator. Smart Materials and Structures, 22(12), 125028.

[39] Fan Yimin, Ghayesh Mergen H, and Lu Tien-Fu. (2021). A broadband magnetically coupled bistable energy harvester via parametric excitation. Energy Conversion and Management, 244, 114505.

[40] Nguyen Minh Sang, Yoon Yong-Jin, and Kim Pilkee. (2019). Enhanced broadband performance of magnetically coupled 2-DOF bistable energy harvester with secondary intrawell resonances. International Journal of Precision Engineering and Manufacturing-Green Technology, 6(3), 521-530.

[41] Tang Xiudong, and Zuo Lei. (2011). Enhanced vibration energy harvesting using dual-mass systems. Journal of Sound and Vibration, 330(21), 5199-5209.

[42] Wu Shuai, Luk Patrick Chi-Kwong, Li Chunfang, Zhao Xiangyu, Jiao Zongxia, and Shang Yaoxing. (2017). An electromagnetic wearable 3-DoF resonance human body motion energy harvester using ferrofluid as a lubricant. Applied Energy, 197, 364-374.

[43] Fan Yimin, Ghayesh Mergen H, and Lu Tien-Fu. (2022). High-efficient internal resonance energy harvesting: Modelling and experimental study. Mechanical Systems and Signal Processing, 180, 109402.

[44] Fan Yimin, Ghayesh Mergen H, Lu Tien-Fu, and Amabili Marco. (2022). Design, development, and theoretical and experimental tests of a nonlinear energy harvester via piezoelectric arrays and motion limiters. International Journal of Non-Linear

Mechanics, 142, 103974.
[45] Wang Guangqing, Liao Wei-Hsin, Yang Binqiang, Wang Xuebao, Xu Wentan, and Li Xiuling. (2018). Dynamic and energetic characteristics of a bistable piezoelectric vibration energy harvester with an elastic magnifier. Mechanical Systems and Signal Processing, 105, 427-446.
[46] Harne RL, and Wang KW. (2015). Dipteran wing motor-inspired flapping flight versatility and effectiveness enhancement. Journal of the Royal Society Interface, 12(104), 20141367.
[47] Zhang Jingyu, Li Xuefeng, Feng Xingxing, Li Renfu, Dai Lu, and Yang Kai. (2021). A novel electromagnetic bistable vibration energy harvester with an elastic boundary: Numerical and experimental study. Mechanical Systems and Signal Processing, 160, 107937.
[48] Ong Zhi Chao, Huang Yu-Hsi, and Chou Sheng-Lun. (2019). Resonant Frequency Reduction of Piezoelectric Voltage Energy Harvester by Elastic Boundary Condition. Journal of Mechanics, 35(6), 779-793.
[49] Zhou Jiaxi, Zhao Xuhui, Wang Kai, Chang Yaopeng, Xu Daolin, and Wen Guilin. (2021). Bio-inspired bistable piezoelectric vibration energy harvester: Design and experimental investigation. Energy, 228, 120595.